AIAA JOURNAL
Vol. 36, No. 7, July 1998

Flame Structure Interactions and State Relationships in an Unsteady Partially Premixed Flame

Suresh K. Aggarwal* and Ishwar K. Puri†
University of Illinois at Chicago, Chicago, Illinois 60607-7022

In this investigation our objective is 1) to compare the similitude between an unsteady, two-dimensional (axisymmetric), partially premixed flame and an analogous steady, partially premixed flamelet to determine if state relationships in terms of a modified conserved scalar apply and 2) to investigate flame structure interactions between the various reaction zones contained in partially premixed flames. This comparison is of fundamental importance to the understanding and modeling of turbulent flames because the axisymmetric flame involves relatively complex flow chemistry interactions resulting from differential diffusion, flame curvature, and spatiotemporally varying strain rates, whereas the development of state relationships generally assumes negligible differential diffusion effects. A time-dependent, axisymmetric model based on a direct numerical simulation methodology using a relatively detailed CH_4–air chemical mechanism is employed to model inverse axisymmetric partially premixed flames that are established by introducing a fuel-rich (CH_4–air) annular jet that is sandwiched between an air jet (on the inside) and coflowing air (on the outside). The flame consists of distinct layers that include 1) an inner layer (PF) in which methane and O_2 consumption occur and 2) an oxidation layer (NF). The broadened inner premixed flame is synergistically coupled with an oxidation layer, and the upstream region of the nonpremixed flame is contained downstream of the premixed flame. The significant hydrocarbon chemistry occurs almost solely in the PF where fuel and radical consumption produce CO and H_2, which are then oxidized to form CO_2 and H_2O in the NF. The nonpremixed flame provides radicals to accelerate the upstream region of the premixed flame. Comparison with an analogous flamelet reveals that transport effects in the axisymmetric flame are significant on the rich side. The coannular flame scalar profiles show regions of both frozen flow and burning. The scalar distributions in the flame, when compared with analogous flamelet profiles, indicate that upstream interactions occur 1) in the rich region with the consequence of enhanced heat release, 2) at the nonpremixed interface leading to higher heat release through H_2 and CO oxidation, and 3) in the lean region where methane consumption occurs despite the local equivalence ratios being well below the lean flammability limit. The synergistic interactions between the inner and outer layers lead to the formation of complex composite flames.

Introduction

USING partially premixed combustion (established, for example, by flowing a jet of fuel-rich mixture in air), one can exploit the advantages of both nonpremixed and premixed flames regarding safety, lower pollutant emission levels, and flame stability. The characteristics of partially premixed flames are also relevant to the liftoff phenomena associated with nonpremixed jet flames, and to turbulent nonpremixed combustion, which can involve regions of partially premixed burning due to local extinction, followed by partial premixing and reignition. Previous investigations of partially premixed flames have employed counterflow-flame and jet-flame configurations.[1–9] The earlier studies of Yamaoka and Tsuji[2–4] established that, depending on the stoichiometry of the premixed stream, two separate reaction zones (or double flames) could be formed. By varying the stretch and partial premixing, Rogg et al.[5] observed that the partial premixing of laminar diffusion flamelets is essential for the prediction of turbulent flame structure. Under certain conditions partial premixing of the reactant streams has been shown to make flames less resistant to stretch and to exhibit both a nonpremixed and premixed-like structure.[7] Yule et al.[10] varied the equivalence ratio of a propane fuel jet between ∞ (nonpremixed flame) and 1.5, i.e., approaching premixed conditions, and the Reynolds number based on the jet characteristics between 3×10^3 and 1.5×10^4 to separate the effects due to fluid mechanics and the combustion phenomena in the flame. Increasing the jet equivalence ratio was found to decrease the thickness of the preheat zone situated between an inner and an outer layer, and higher levels of partial premixing were found to increase the frequency at which instabilities occurred.

We have found the flame structure of unsteady partially premixed jet-like methane–air flames to be different from that of typical nonpremixed laminar jet flames.[11,12] Our investigations have revealed that, once oxygen is depleted inside an inner rich region, nonpremixed flames are established in an outer region once excess fuel and partially oxidized products emerge from the premixed zone into this nonpremixed zone. Methane consumption in the premixed flame occurs through the reaction $CH_4 + H \Leftrightarrow CH_3 + H_2$, and methyl radicals are converted to CH_2O, which forms CHO and eventually CO. The carbon monoxide and molecular hydrogen formed due to premixed combustion provide the fuel for nonpremixed flames established as a result of partial oxidation in the premixed flame. Oxygen consumption in the nonpremixed region is due to the reaction $H + O_2 + M \Leftrightarrow HO_2 + M$. The HO_2 is rapidly consumed to form OH radicals that, in turn, are responsible for H_2 and CO oxidation.

In this study, we investigate the flame structure of transient partially premixed flames to determine whether state relationships in terms of a modified conserved scalar apply. The structure of inverse partially premixed flames established by introducing a fuel-rich (CH_4–air) annular jet sandwiched between an axisymmetric air jet (on the inside) and coflowing air (on the outside) is predicted through computations. A time-dependent, axisymmetric model based on a direct numerical simulation methodology is employed, and a relatively detailed 52-step mechanism proposed by Peters[13] is used to model the CH_4–air chemistry.

The chemical structure and dominant reaction pathways have been discussed in an earlier publication.[12] The present investigation focuses on the chemical and fluid dynamic interactions between the premixed flame in the upstream region and the downstream nonpremixed flame. Our second objective is to compare the similitude between an unsteady, two-dimensional (axisymmetric), partially premixed flame and analogous partially premixed flamelets. This comparison is of fundamental importance to the understanding

Received Aug. 23, 1997; revision received Feb. 15, 1998; accepted for publication March 9, 1998.

*Professor, Department of Mechanical Engineering (M/C 251), 842 W. Taylor Street, RM 2039. E-mail: ska@uic.edu. Associate Fellow AIAA.

†Associate Professor, Department of Mechanical Engineering (M/C 251), 842 W. Taylor Street, RM 2039. E-mail: ikpuri@uic.edu. Member AIAA.

and modeling of turbulent flames because the axisymmetric flame involves relatively complex flow chemistry interactions resulting from differential diffusion, flame curvature, and spatiotemporally varying strain rates. On the other hand, flamelets are thin in both spatial and mixture fraction coordinates, locally one dimensional, and characterized by relatively fast chemistry with simpler flow chemistry interactions that occur through the imposition of a specified strain rate.

Although the effects of varying strain rates and the chemistry are readily investigated using steady flamelets, more complex effects due to spatially and temporally varying strain rates, varying spatial flame thickness, multidimensional transport of heat and radicals, and local flame extinction and reignition can only be investigated in unsteady and/or multidimensional flames. Sivathanu and Faeth[14] have found that state relationships are generally applicable for the major species (N_2, O_2, fuel, CO_2, and H_2O) found in nonpremixed hydrocarbon–air flames. Their analysis considered various configurations over a range of strain rates. These relationships depart from equilibrium predictions because of effects due to finite rate chemistry.

Physical-Numerical Model

The flow configuration on which the computational study is based is schematically depicted in Fig. 1. A vertically mounted axisymmetric flame is established by injecting a fuel-rich CH_4–air mixture from an annular ring between an axisymmetric air jet on the inside and coflowing air on the outside. The inner and outer diameters of the annular ring are 9.9 and 12.7 mm, respectively. The combustion process is simulated by employing a detailed numerical model based on the solution of time-dependent governing equations for an axisymmetric reacting flow.

Using cylindrical coordinates (z, r), we can write the governing equations in the form

$$\frac{\partial(\rho\phi)}{\partial t}+\frac{\partial(\rho u\phi)}{\partial z}+\frac{\partial(\rho v\phi)}{\partial r}=\frac{\partial}{\partial z}\left(\Gamma^{\phi}\frac{\partial\phi}{\partial z}\right)+\frac{\partial}{\partial r}\left(\Gamma^{\phi}\frac{\partial\phi}{\partial r}\right)-\frac{\rho v\phi}{r}+\frac{\Gamma^{\phi}}{r}\frac{\partial\phi}{\partial r}+S^{\phi}$$

where ρ represents the density and u and v represent the axial and radial velocity components, respectively. The general form of the preceding equation represents either of the mass, momentum, species, or energy conservation equations. The transport coefficient Γ^{ϕ} and the source terms S^{ϕ} appearing in the governing equations are provided in Table 1, for which p denotes pressure; μ, λ, and c_p are, respectively, the viscosity, thermal conductivity, and specific heat of the mixture; g is the gravitational acceleration; ρ_o is the density of air; $\dot{w}_i$ is the mass production rate of the ith species; and D_{i-N_2} is the diffusion coefficient of ith species in a binary

Table 1 Transport coefficients and source terms appearing in governing equations

Equations	Φ	Γ^{Φ}	S_g^{Φ}
Continuity	1	0	0
Axial momentum	u	μ	$-\frac{\partial p}{\partial z}+(\rho_o-\rho)g+\frac{\partial}{\partial z}\left(\mu\frac{\partial u}{\partial z}\right)+\frac{\partial}{\partial r}\left(\mu\frac{\partial v}{\partial z}\right)+\frac{\mu}{r}\frac{\partial v}{\partial z}-\frac{2}{3}\left[\frac{\partial}{\partial z}\left(\mu\frac{\partial u}{\partial z}\right)+\frac{\partial}{\partial z}\left(\mu\frac{\partial v}{\partial r}\right)+\frac{\partial}{\partial z}\left(\mu\frac{v}{r}\right)\right]$
Radial momentum	v	μ	$-\frac{\partial p}{\partial r}+\frac{\partial}{\partial z}\left(\mu\frac{\partial u}{\partial r}\right)+\frac{\partial}{\partial r}\left(\mu\frac{\partial v}{\partial r}\right)+\frac{\mu}{r}\frac{\partial v}{\partial r}-2\mu\frac{v}{r^2}-\frac{2}{3}\left[\frac{\partial}{\partial r}\left(\mu\frac{\partial u}{\partial z}\right)+\frac{\partial}{\partial r}\left(\mu\frac{\partial v}{\partial r}\right)+\frac{\partial}{\partial r}\left(\mu\frac{v}{r}\right)\right]$
Species mass fraction	Y_i	ρD_{i-N_2}	$\dot{w}_i$
Energy	H	$\frac{\lambda}{C_p}$	$\nabla\left\{\frac{\lambda}{c_p}\sum_1^{N_s}\left[\left(Le_i^{-1}-1\right)H_i\nabla Y_i\right]\right\}-\sum_1^{N_s}\left(h_{fi}^{o}\dot{w}_i\right)$

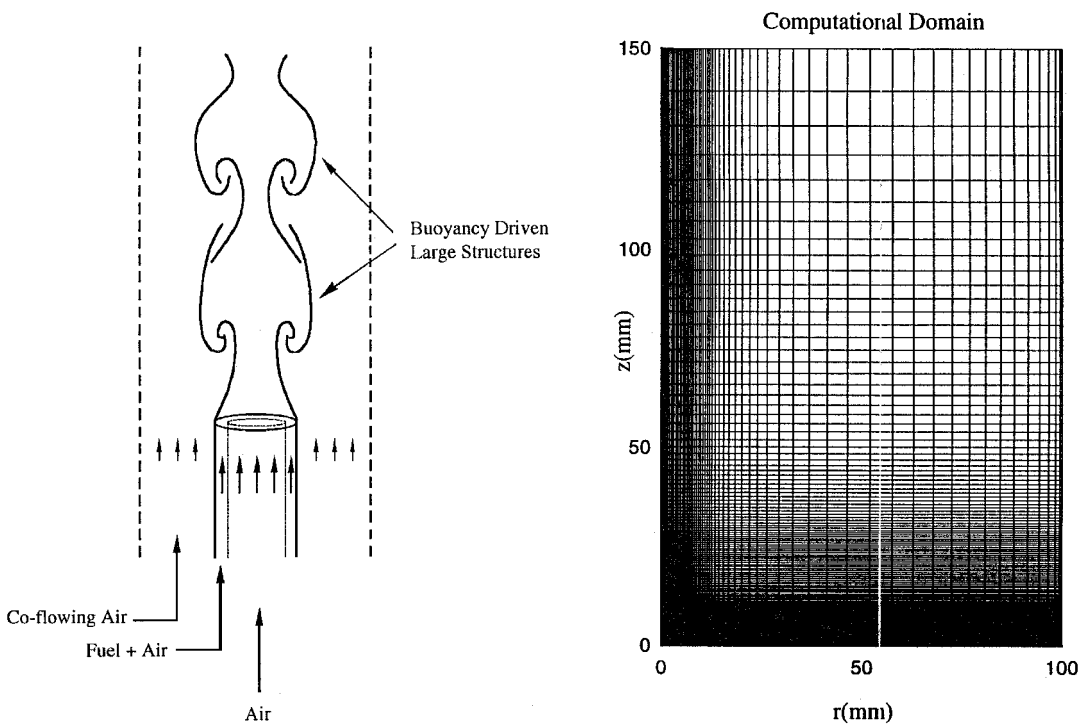

Fig. 1 Schematic of a methane–air inverse diffusion flame.

mixture of that species and nitrogen and H the enthalpy. Finally, $Le_i = \lambda/(\rho D_{i-N_2} c_p)$ denotes the Lewis number of species i. The set of governing equations is completed by using the overall species conservation equation and the equation of state. The thermodynamic and transport properties are considered to be temperature and species dependent. A detailed algorithm, similar to that in CHEMKIN,[15] is employed to calculate these properties.

A multistep mechanism is employed to represent the CH_4–air chemistry in these detailed calculations. It involves 52 elementary reactions and 17 species (CH_4, O_2, CH_3, CH_2, CH, CH_2O, CHO, CO_2, CO, H_2, H, O, OH, H_2O, HO_2, H_2O_2, N_2), the rates for which can be found in Ref. 14.

Boundary Conditions

In the following section, the flame structure of a representative unconfined axisymmetric methane–air flame established at a Froude number $Fr = 0.5$, Reynolds number $Re = 5 \times 10^2$, and overall equivalence ratio $\phi = 1$ at atmospheric pressure will be discussed. The Froude and Reynolds numbers are based on the dimensions and exit velocity of the inner air jet. The overall equivalence ratio in the flow (considering both fuel-rich and pure oxidizer zones) is stoichiometric, i.e., $\phi = 1$, and that issuing from the annular ring is $\phi_r = 2.5$. The inlet temperature is 294 K everywhere, and the gravitational acceleration is set at 6 g. The computational conditions are as follows.

1) In the domain, a) the inner and outer duct radii (R_I and R_O) are, respectively, 0.494 and 0.635 cm; and b) the domain radius and length (R_C and Z) are, respectively, 10 and 15 cm, with the locations $r = 0$ and $z = Z$, respectively, representing the axis and free surface.

2) The inlet ($z = 0$) conditions are given by the following: a) for $r < R_I$, the oxygen and methane mass fractions (Y_{O_2} and Y_{CH_4}) are, respectively, 0.24 and 0, and the radial and axial velocities (U_r and U_z) are, respectively, 0 and 0.61 m s^{-1}; b) for $R_I < r < R_O$, $Y_{O_2} = 0.203$, $Y_{CH_4} = 0.127$, $U_r = 0$ m s^{-1}, and $U_z = 0.61$ m s^{-1}; and c) for $R_O < r \leq R_C$, $Y_{O_2} = 0.23$, $Y_{CH_4} = 0$, $U_r = 0$ m s^{-1}, and $U_z = 0.05$ m s^{-1}.

Numerical Method

An implicit algorithm is employed to solve the unsteady gas-phase equations. The governing equations are integrated by using a finite control volume approach with a staggered, nonuniform grid system.[16,17] Grid lines are clustered near the flame surfaces to resolve the steep gradients of the dependent variables. Boundaries of the computational domain are shifted sufficiently to minimize the propagation of disturbances into the region of interest. An iterative alternative direction implicit technique is used for solving the resulting ($N_s + 3$) sets of algebraic equations. A stable numerical-integration procedure is achieved by coupling the species and energy equations through the chemical-reaction source terms. At every time step, the pressure field is calculated by solving the pressure Poisson equations at all grid points simultaneously and utilizing the lower and upper diagonal matrix-decomposition technique.

Further details about the numerical procedure, treatment of boundary conditions, and validation studies are provided in earlier publications.[17–21] First, a steady-state solution is obtained by using a global one-step mechanism. Subsequently, this solution is employed as the initial condition for the detailed-chemistry unsteady calculations. Soon thereafter, following a sufficient time period, the influence of the initial one-step chemistry on the unsteady solutions becomes negligible.

Discussion

Generic Partially Premixed Flame Structure

A generic partially premixed flame consists of two streams with, respectively, rich and lean side equivalence ratios ϕ_r and ϕ_1, where $1 < \phi_r < \infty$ and $0 < \phi_1 < 1$ (Ref. 22). For most applications, the global stoichiometry based on both the rich and lean streams will be either stoichiometric or overall fuel lean. For stoichiometric combustion, both premixed ($\phi_r = 1$ and $\phi_1 = 0$) and nonpremixed flames ($\phi_r \to \infty$ and $\phi_1 = 0$) correspond to specific levels of partial premixing. The flame structure of partially premixed hydrocarbon flames can be similar to that of premixed flames, except for the oxidation layer chemistry, because complete oxidation of CO and H_2 is oxidizer transport limited. For cases when $\phi_r \gg 1$ and $\phi_1 = 0$, the flame structure is expected to be similar to that of nonpremixed flames, except for the influence of certain premixed-type initiation reactions that occur in the very rich region. Furthermore, in such cases state relationships should be possible because the lean conditions $\phi_1 \to 0$ approach thermodynamic equilibrium in a manner similar to nonpremixed flames,[14] and the rich side $\phi_r \gg 1$ involves relatively passive mixing that is perturbed by the initiation reactions as $\phi_1 \to 1$.

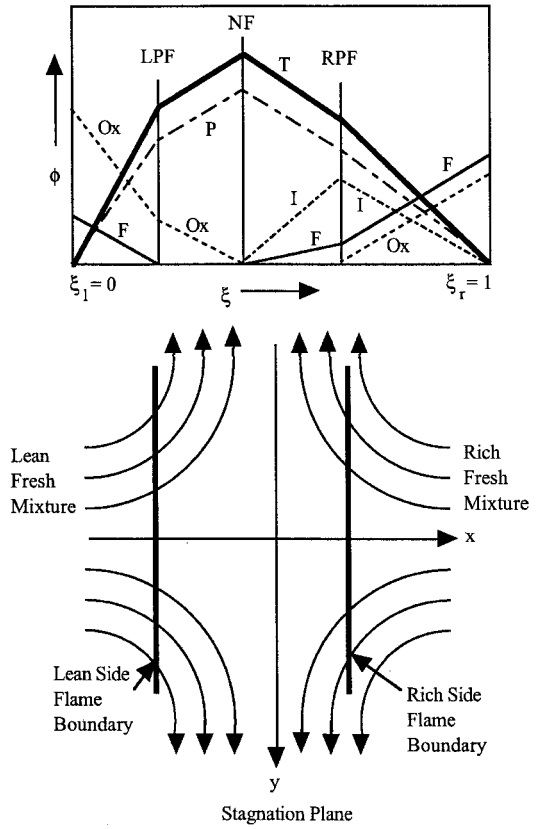

Fig. 2 Schematic illustration of the generic flame structure of partially premixed flames. Generic state relationships for the scalar profiles are presented with respect to a modified conserved scalar.

To determine the existence of the state relationships, the flame structure of partially premixed flames can be compared in different configurations by considering the scalar profiles with respect to a modified conserved scalar $\xi = (Z - Z_1)/(Z_r - Z_1)$ (Ref. 22). Here Z denotes the relative local mass fraction originating in the fuel, and the subscripts r and 1 are conditions relevant at the boundaries of the rich and lean regions, respectively. Use of ξ transforms the system-specific spatial coordinate system into a generic, universally applicable coordinate. In a generic partially premixed flame, the lean side equivalence ratio (at $\xi = 0$) is ϕ_1, and the rich side ratio (at $\xi = 1$) is ϕ_r. Figure 2 contains a schematic illustration of the generic flame structure in the context of a counterflow flame. State relationships for the scalars are depicted in terms of a modified mixture fraction.

Unsteadiness

The high temperatures lead to buoyant convection on both sides of the flame, and toroidal vortices periodically roll up due to the convective Kelvin–Helmholtz instabilities. It is important to note that the unsteady flame simulated in the present study is periodic with well-organized vortex structures. The simulation of such flames is not dependent on the intial conditions. The flame/plume structure can be inferred from the instantaneous temperature contours and velocity vectors presented in Fig. 3 at four different times. Flow unsteadiness includes the following dynamic sequence of events: 1) The vortex rolls up in both the outer and inner flow due to which two vortex rings are simultaneously generated; 2) the vortices convect

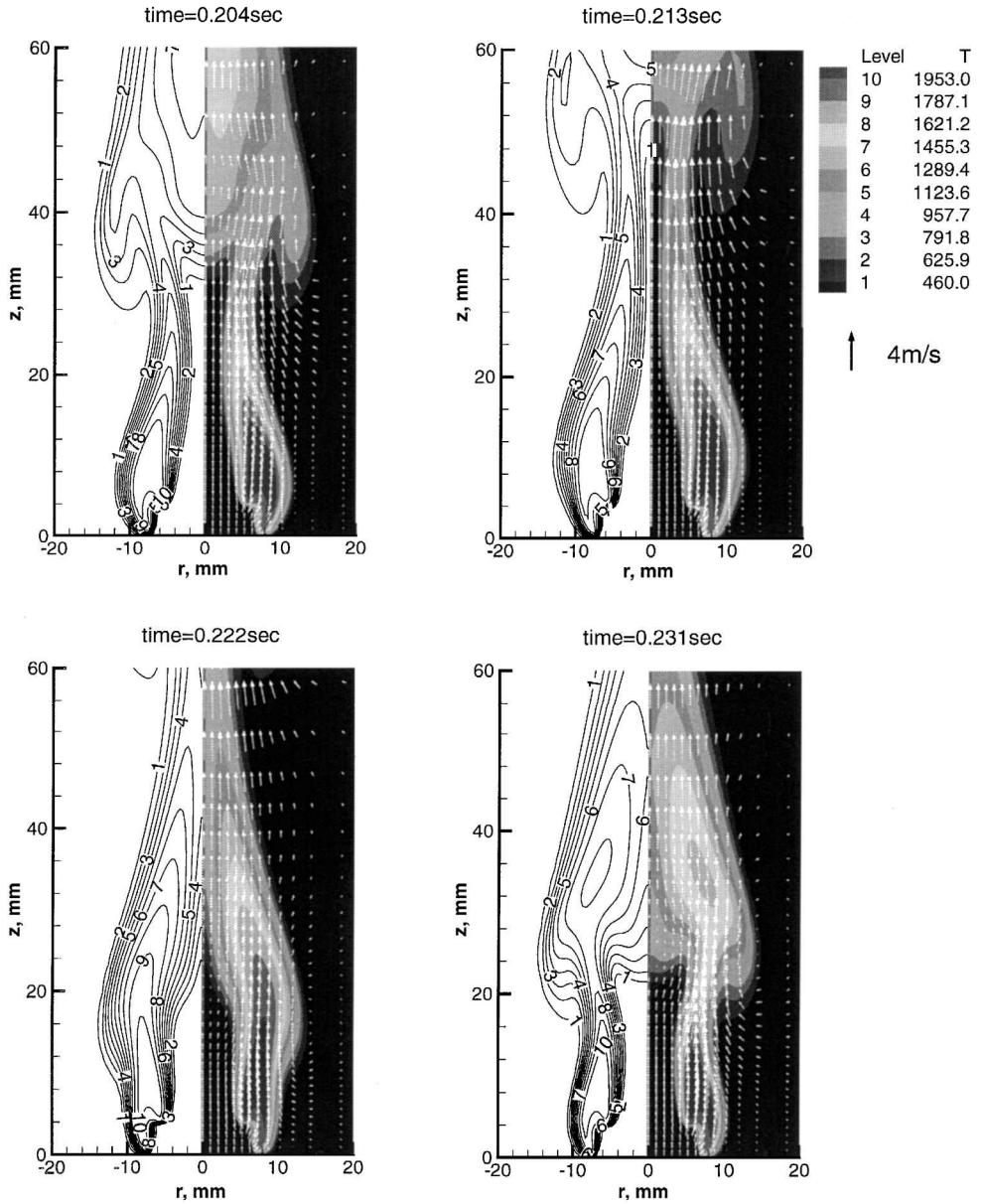

Fig. 3 Instantaneous velocity vectors and temperature profiles for a flame established at $Fr = 0.5$, $Re = 5 \times 10^2$, and overall $\phi = 1.0$ at four different times.

downstream; 3) the vortices interact with the two high-temperature surfaces, squeezing and bulging them; and 4) this leads to pinchoff and flicker. This double-vortex structure associated with two flame surfaces is a unique feature of the inverse partially premixed flame, which, to the best of our knowledge, has not been previously observed.

Predicted Flame Structure

The flame structure is obtained in the form of instantaneous snapshots of the flow at various times. In the fuel-rich annular ring, the flame initiation process is dominated by premixed combustion close to the nozzle exit. As oxygen is depleted inside the annular ring, the excess fuel emerging from the fuel-rich premixed zone is transported outward (by convection and diffusion), and nonpremixed flames are established on both sides of the annular ring. The two high-temperature product regions later merge into a single surface in the plume. Subsequently, the buoyant acceleration of hot gases outside the diffusion flame surface causes shear layer rollup, leading to the formation of toroidal vortex rings, which then interact with the flame/plume surface.[11] The flame/plume structure depicted in Fig. 3 is periodic. Consequently, the time interval between two consecutive snapshots in the figure is chosen to be roughly one-fourth of the vortex time period (≈36 ms), which is defined as the inverse of the flickering frequency.

The global flame structure of the unsteady flame is schematically depicted in Fig. 4. A rich reactant core ($\phi_r = 2.5$) is flanked by two separate oxidizer streams ($\phi_1 = 0$) that emerge with different initial velocities. An inner premixed flame is surrounded by two nonpremixed flames, and the overall flame structure can be characterized as follows[12]: 1) CH_4 and O_2 react with atomic hydrogen in the premixed flame (through the initiation reaction $CH_4 + H \Leftrightarrow CH_3 + H_2$) and provide CO and H_2, and 2) carbon monoxide and molecular hydrogen are oxidized in the nonpremixed flame by hydroxyl radicals to form CO_2 and H_2O (through the reactions $CO + OH \Leftrightarrow CO_2 + H$ and $H_2 + OH \Leftrightarrow H_2O + H$). The two oxidation reactions provide the H atoms 1) that are recycled through O_2 to form OH (i.e., by the combined effect of reactions $H + O_2 + M \Leftrightarrow HO_2 + M$ and $HO_2 + H \Leftrightarrow OH + OH$) and 2) that initiate the reactions in the premixed flame. Hydroxyl radicals are also produced throughout the flame through the reaction $H + O_2 \Leftrightarrow OH + O$.

The basic structure of the flame can be assumed to consist of distinct layers[23–26] that include 1) an inner layer (PF) in which methane and O_2 consumption occur and 2) an oxidation layer (NF) (surrounded by a preheat zone downstream of PF and a postflame zone downstream of NF). All of the hydrocarbon chemistry can be assumed to occur in the inner layer where fuel and radical consumption occurs to form CO and H_2. In the oxidation layer, the CO and

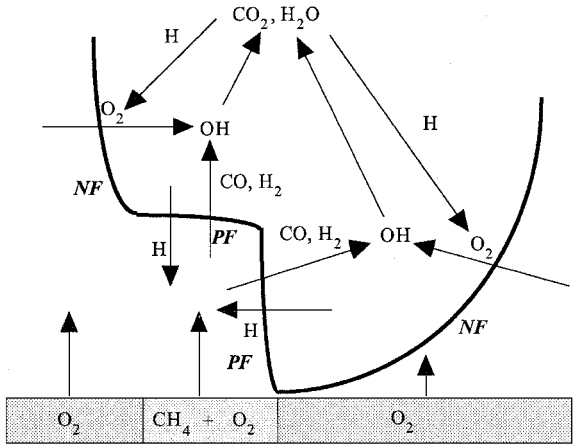

Fig. 4 Schematic description of the global flame structure of a generic partially premixed flame. PF and NF, respectively, denote the premixed and nonpremixed flame regions. The left-hand portion of the flame is raised because the oxidizer-stream velocity there is higher. The oxidizer-stream velocity on the right-hand side is lower and allows flame stabilization at a lower location.

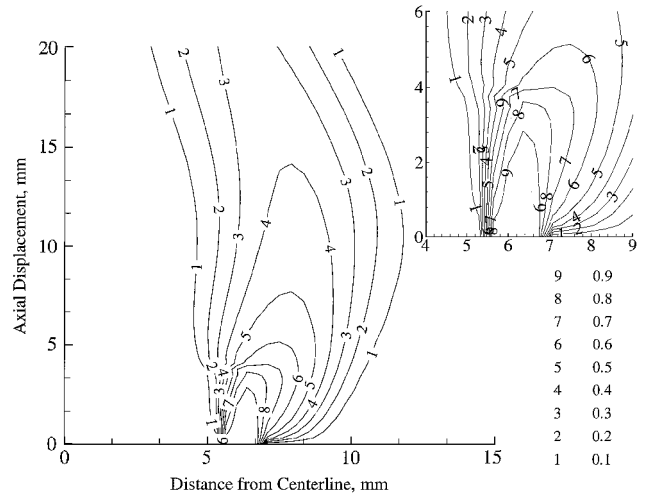

Fig. 5 Contours of the modified mixture fraction ξ for the flame corresponding to Fig. 3a.

H_2 formed in the inner layer are oxidized to form CO_2 and H_2O. The CO-oxidation layer is generally thicker than the H_2-oxidation layer, and the overall thickness of the oxidation layer itself is, in general, greater than that of the inner layer. Furthermore, the heat release is primarily due to the exothermic reactions occurring in the oxidation layer. A major exothermic reaction in the oxidation layer (NF) $CO + OH \Leftrightarrow CO_2 + H$ occurs on a relatively slower timescale than either the initiation reactions in the inner layer (PF), e.g., $CH_4 + H \Leftrightarrow CH_3 + H_2$, or the other major oxidation reaction in the NF, namely, $H_2 + OH \Leftrightarrow H_2O + H$ (Ref. 27).

A major distinction between the structures of partially premixed and analogous nonpremixed and premixed flames is due to the synergistic interactions occurring between the PF and NF layers. Unlike in a premixed flame, the oxidation reactions in partially premixed flames are rate limited by transport of additional ambient oxygen into the oxidation layer. Perturbations in that transport should affect not only the oxidation layer (through the exothermic reactions involving CO and H_2) but also the inner layer because the outer oxidation region provides H atoms (and heat transport) to initiate the reactions that occur in the inner core. Sohrab et al.[28] have classified the interaction between flames into two categories, namely, upstream and downstream interactions. During upstream interactions the preflame regions of flames interact synergistically, so that heating and/or radical sharing can lead to the acceleration of one or both flames. Downstream interactions are more subtle and complex and involve thermal and/or chemical interaction(s) between the postflame zones of various flames. The partially premixed flames considered herein undergo an upstream-type of interaction because the radical pools and thermochemistry in the two flames are synergistically coupled as the nonpremixed flame provides radicals to accelerate the upstream region of the premixed flame.

Flamelet Comparison

The laminar flamelet model of turbulent combustion is applicable to both premixed and nonpremixed combustion characterized by fast chemistry and requires that the flamelets be thin.[29] Although premixed flamelets are required to be spatially thin, the relevant coordinate for analysis of nonpremixed flamelets is the mixture fraction. For the partial premixing conditions of this investigation, i.e., characterized by $\phi_r = 2.5$, and $\phi_1 = 0$, the nonpremixed flame is an important synergistic component of the system. Therefore, in the context of the laminar flamelet model, it is of interest to characterize the flame in terms of the modified conserved scalar ξ. Because nitrogen has been found to mix passively and to follow a generalized state relationship in hydrocarbon–air flames, it is appropriate to define ξ on the basis of the nitrogen elemental mass fraction. However, we have found that the ξ contours for the flame are relatively insensitive to choice of element, except in the rich-side premixed reaction zone.

Figure 5 contains the nitrogen-based ξ contours for the unsteady axisymmetric partially premixed flame shown in Fig. 3a that map the region between the lean ($\xi \to 0$) and rich ($\xi \to 1$) portions of the flame. In a manner similar to that employed for nonpremixed flames, the local strain rate can be represented in the form of the local scalar dissipation rate[5] that is proportional to $(\nabla\xi \cdot \nabla\xi)$. Figure 5 shows that the ξ isocontours around $r = 5.5$ mm are clustered in close proximity, especially for the inner flow for small axial displacements. Because the scalar dissipation rate is high at these locations, the chemistry there is frozen. Therefore, the inner flame establishes itself not at the nozzle exit but at an upstream location, as is schematically illustrated in Fig. 4. Because the two-dimensional flame experiences a range of local strain rates, the flamelet strain rate response will be illustrated by investigating the analogous counterflow flames.

The counterflow geometry is well suited to establish flames that can be mapped into mixture fraction space.[22,29] Downstream interactions can be clearly established and investigated in the counterflow geometry, e.g., with two flames being established on either side of a stagnation plane (see also Fig. 2). Upstream interactions, which might occur in two- or three-dimensional flows due to varying local strain rates, molecular transport of heat and radicals, and local attachment of the flames, are not readily investigated in this geometry (although they can occur in the context of two flames established on the same side of the stagnation plane). To understand the applicability (or limitations) of the flamelet model (and of state relationships), we compare the structure of the computed two-dimensional flame with that of a representative flamelet.

Numerical simulations of strained partially premixed flames were performed using a previously developed computer code[30] that employs a detailed model of both the molecular transport of chemical species and the chemical reaction schemes.[31] The chemical kinetic scheme is taken from the literature. It includes 278 elementary forward and backward reactions and involves 30 gas-phase species, including C_2-hydrocarbons.[32] Validation of the counterflow calculations with experimental results is to be found in Ref. 33. Because of computational limitations in the case of the unsteady multidimensional flame, its chemistry is less complex (with the C_2 chemistry being neglected) than that of the counterflow flamelet. Consequently, in the present investigation the chemical characterization of the flamelet is more accurate than that of the unsteady coflow flame. Therefore, in addition to transport effects, a comparison of the flame structures will also reveal differences based on chemistry, and the results are expected to elucidate the significant chemical differences that arise due to this computational constraint.

State Relationships

Spatial multidimensionality can induce locally varying 1) spatial flame thickness, 2) strain rates, and 3) molecular transport. Therefore, deviations in the flame structures of the unsteady axisymmetric and laminar flamelets may be pronounced because although an individual flamelet is characterized by a distinct strain rate (therefore,

a specific consumption rate), the unsteady axisymmetric flame is an ensemble of several flamelets established at various strain rates. The modified mixture fraction is based on the assumption of equal molecular diffusivities for all species.

The counterflow simulations considered a laminar methane–air mixture ($\phi_r = 2.5$) impinging on a laminar stream containing pure air ($\phi_1 = 0$), both streams being introduced through opposed jets. This stoichiometry matches that of the streams emerging from the annular jet in the unsteady calculations. It was not possible to obtain stable solutions past a strain rate of 290 s^{-1}, which is, therefore, interpreted as being close to the critical extinction strain rate. In Figs. 6a–6c, the counterflow flamelet structure is presented over a range of strain rates corresponding from moderate (50 s^{-1}) to near extinction (290 s^{-1}).

Figures 6a–6c show that, as expected, once the strain rate increases, the flame thickness decreases, the oxygen leakage across the flame increases, the fuel consumption in it declines, and CO oxidation to CO_2 is reduced. The oxygen and methane concentrations are sensitive to strain rate in the region $\xi \approx 0.5$–0.6 where the chemistry occurs. In the context of Fig. 2, the intermediate species CO and H_2 are formed in the rich premixed flame (RPF), and fuel is completely consumed in the NF. However, their state relationships are applicable over a wide range of ξ. The state relationships for N_2, CO_2, and H_2O are generally applicable, as are those for OH, which is a radical species. In general, state relationships for the minor species CO and H_2 are also satisfactory, which is significant, because both these minor species take part in the PF–NF chemical interactions, whereas CH_4 and O_2 are consumed in either of these flames. The flamelet thickness decreases spatially by almost a factor of 3 as the strain rate is increased from moderate to near-extinction conditions.

Select flamelet and two-dimensional scalar profiles for the flame corresponding to Fig. 3a are presented in terms of ξ in Figs. 7a–7d. For the sake of brevity, and because the mass fraction profiles of various species do not exhibit dramatic differences, a single flamelet profile corresponding to a moderate strain rate of 50 s^{-1} is presented. We observe from Figs. 7a–7d that the two-dimensional results are well represented by the flamelet calculations. The coannular flame contains regions of both vigorous burning and frozen flow, with a few locations that are either quenched or reignited. The peak temperature in the coannular flame is higher than that in the flamelet, which is attributable both to lower local strain rates in the two-dimensional flame and to transport and chemistry effects. The molecular transport of heat in the coannular flame lags that of the counterflow flame, particularly on the rich ride, and the temperature gradients near the peak temperature in mixture fraction space are steeper. In that sense, the coannular flame is thinner in ξ space than is the counterflow flame.

Transport and chemistry effects are particularly significant on the rich side at $\xi \approx 0.75$. These are probably due to the upstream interaction that occurs between the nonpremixed flame and the rich premixed flame on the right-hand side of the schematic diagram contained in Fig. 4. At this location, small amounts of methane cross the rich reaction zone past the inner rich premixed flame. This is apparent upon examining the methane mass fraction and equivalence ratio contours contained in Figs. 8a and 8b, respectively. On the right-hand sides of these figures, i.e., at $r > 7$ mm, we note that, even though the methane concentration decreases by two orders of magnitude (contours are presented from 10^5–10^3 ppm), the local equivalence ratio ϕ increases from 2.5 to in excess of 50 because oxygen transport into the outer nonpremixed region (NF) is limited. From Fig. 3a we note that the expansion due to the premixed flame at $r \approx 7$ mm pushes the oxygen flow outward, limiting convective mixing. However, even though the absolute methane concentration is small in this region contained between the premixed flame and outer oxidizer flow, fuel radical-based reactions proceed due to thermal transport, forming molecular hydrogen. The H_2, so produced, is oxidized through the heat-releasing reaction $H_2 + OH \Leftrightarrow H_2O + H$, with the result that the local temperature exceeds the counterflow flame temperature at $\xi \approx 0.75$. From Fig. 8b we also observe that the local equivalence ratio is ultralean toward the inner jet core due to transport of methane toward the centerline.

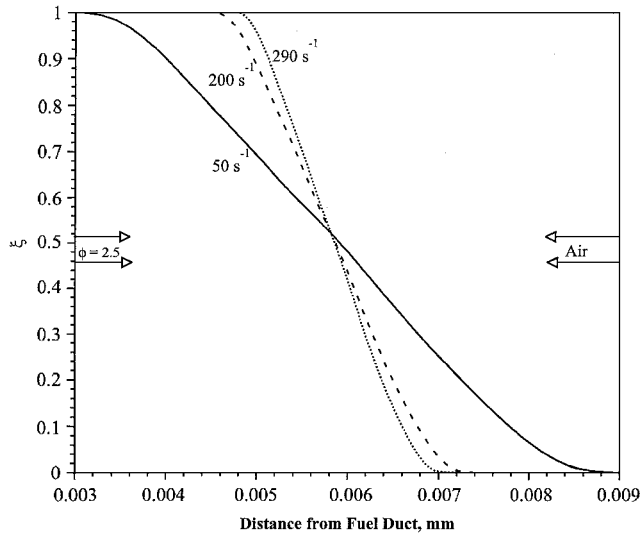

a) Flame thickness in terms of the spatial distribution of ξ

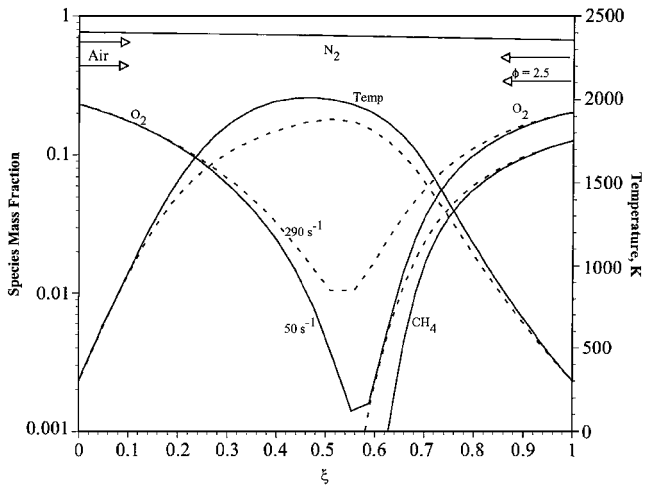

b) Temperature and mass fraction profiles of CH_4, O_2, and N_2

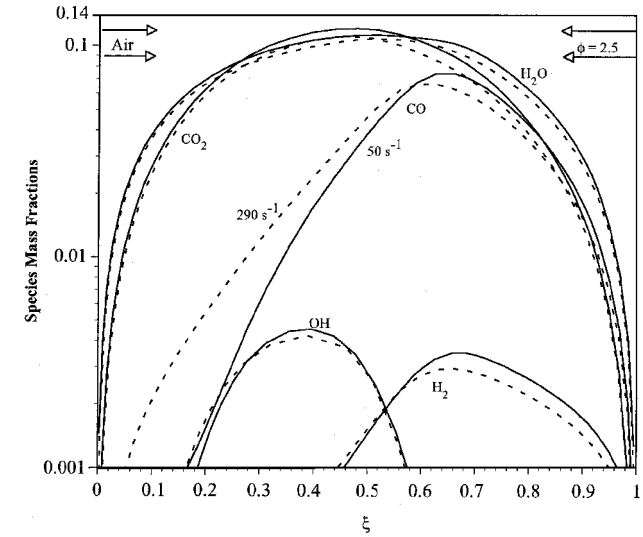

c) Mass fraction profiles of CO_2, H_2O, CO, H_2, and OH

Fig. 6 Flame structure of counterflow flames established by flowing a $\phi_r = 2.5$ methane–air mixture against air at strain rates of 50 and 290 s^{-1}.

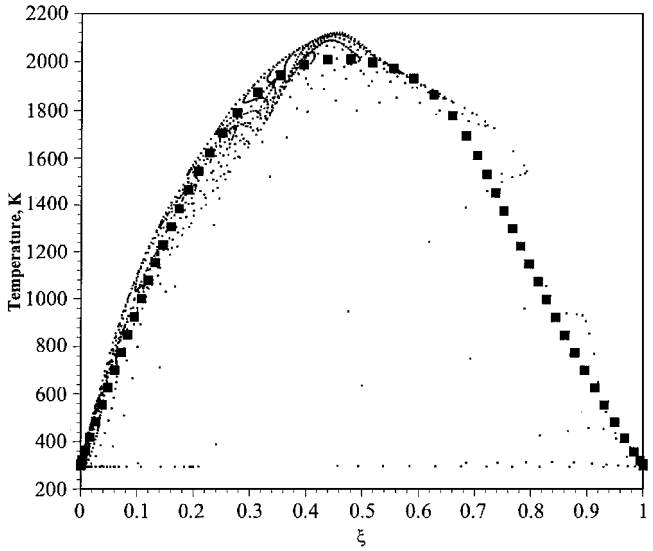

a) Temperature

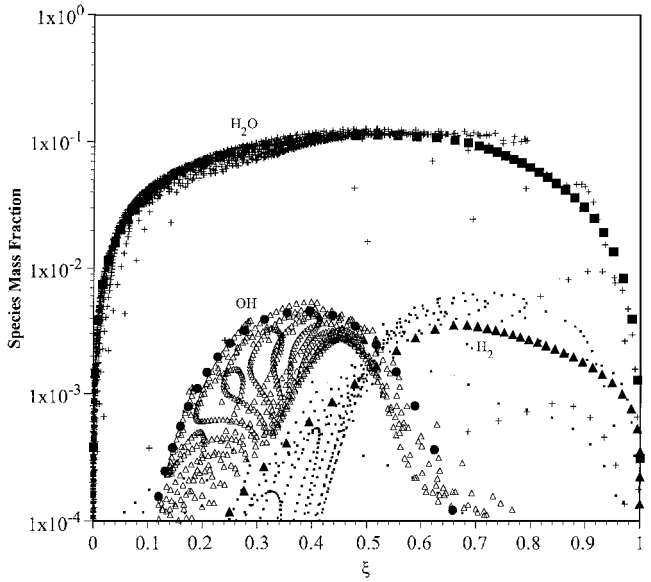

c) H_2 (△, ●), H_2O (+, ■), and OH (■, ▲)

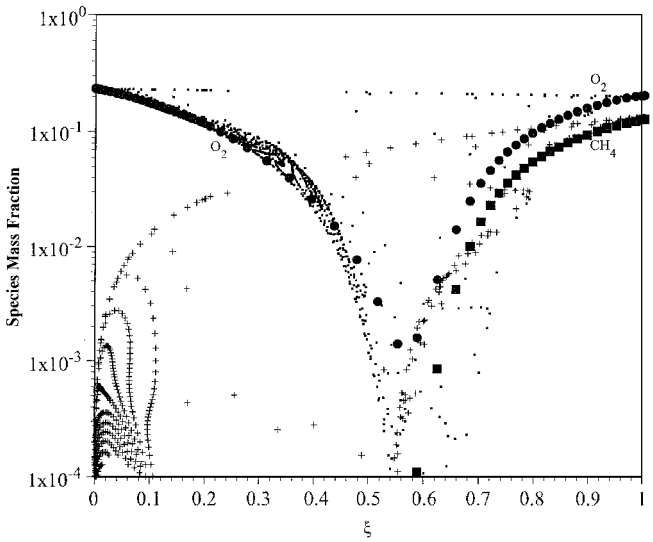

b) O_2 (■, ●) and CH_4 (+, ■)

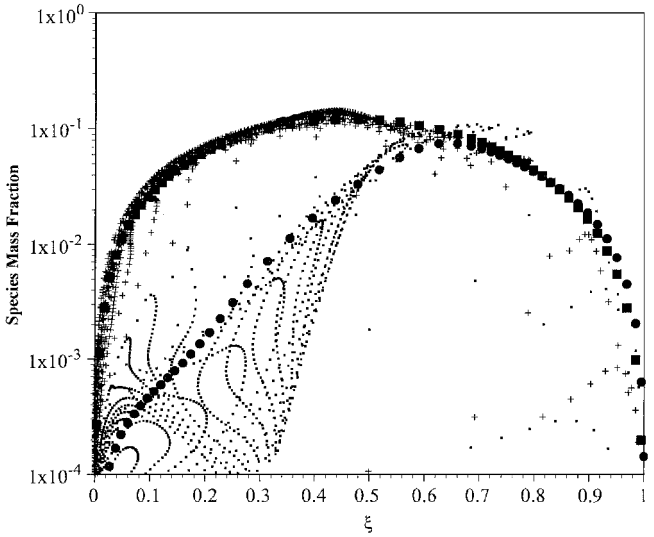

d) CO (■, ●) and CO_2 (+, ■)

Fig. 7 State relationships of scalar profiles with respect to ξ comparing the flame corresponding to Fig 3a with an analogous steady counterflow flame at a moderate strain rate of 50 s^{-1}.

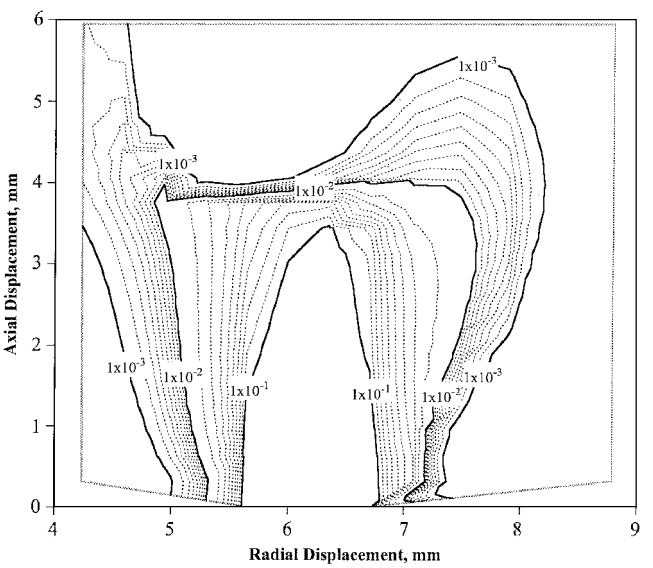

Fig. 8a Contours of the methane mass fraction for the flame corresponding to Fig. 3a.

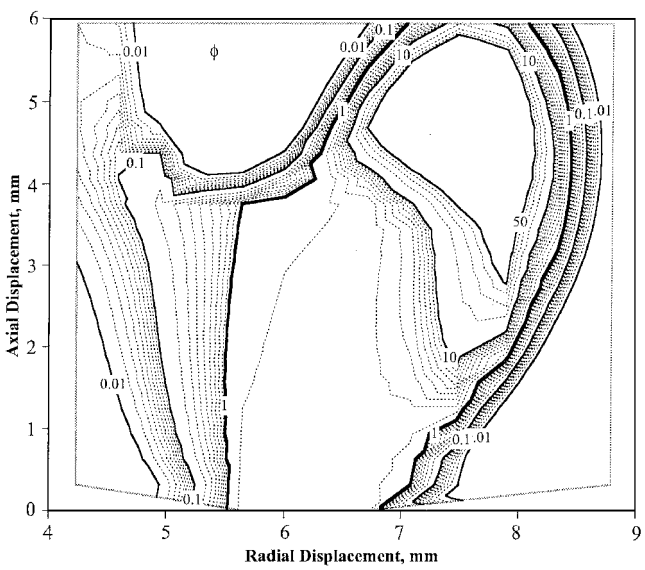

Fig. 8b Contours of the equivalence ratio for the flame corresponding to Fig. 3a.

These phenomena are apparent upon comparing the O_2 and CH_4 profiles for the coannular flame and the counterflow flamelet presented in Fig. 7b. Although oxygen is consumed at a higher rate in the coannular flame as compared with the flamelet due to the lower local strain rates, the concentration profiles for the two cases are qualitatively and quantitatively similar over three orders of magnitude of the O_2 mass fraction. The coannular flame profiles show regions of both frozen flow and burning. The methane mass fraction profile shows evidence of CH_4 consumption in the lean region, i.e., for $\xi < 0.1$. This is due to the aforementioned transport of methane toward the coannular flame centerline. Even though the local equivalence ratio is less than 0.1 for $r < 5$ mm, the heat transported from the rich premixed flame is able to sustain a lean premixed flame. The methane consumption in the lean region leads to CO mass fractions in excess of those in a flamelet for $\xi < 0.2$, as shown in Fig. 7d. Likewise, due to heat transport, O_2 consumption in the rich region $0.55 < \xi < 0.8$ is higher than that predicted by the flamelet profile, leading to higher OH mass fractions as shown in Fig. 7c. The enhanced heat transport in the coannular flame raises the rate of fuel consumption above that in an equivalent flamelet at those locations, and, thereby, the H_2 mass fraction, as shown in Fig. 7c. The larger amounts of molecular hydrogen lead to higher levels of H_2O and heat release as discussed earlier, so that the local flame temperature around the contour $\xi \approx 0.7$ is higher than that for a flamelet.

The enhanced fuel decomposition in the rich ($\xi \approx 0.7$) region leads to a larger CO concentration than exists at a similar location in a flamelet, as shown in Fig. 7d, although for the most part the major product (CO_2 and H_2O) mass fraction profiles follow those computed for the flamelet. Hydroxyl radicals, which play a major role during oxidation and heat release, are bounded in the coannular flame by their flamelet profile. Around $\xi \approx 0.44$, the CO mass fraction at certain spatial locations in the coannular flame is significantly lower than that in the flamelet, implying a higher conversion to CO_2. (A similar observation can be made regarding conversion of H_2 to H_2O around $\xi \approx 0.44$.) Comparing Figs. 7c and 7d, we note that the OH profile in the coannular flame can deviate from the flamelet profile around that location, with the result that the carbon dioxide mass fractions around $\xi \approx 0.44$ lie above the corresponding flamelet values.

In general, the major species (O_2, CH_4, CO_2, and H_2O) exhibit state relationships with respect to the modified mixture fraction, Moreover, the absence of C_2 chemistry in the unsteady axisymmetric calculations does not appear to dramatically impact these relationships. (The departures of the unsteady scalar profiles from their flamelet counterparts in a narrow region on the rich side are most likely due to system-specific transport effects, as discussed earlier.) This information can prove useful in turbulent combustion modeling. These results are in accord with those for steady nonpremixed flames,[34] which found generally excellent agreement between individual species profiles measured in two-dimensional Wolfhard–Parker burners and the corresponding counterflow flame predictions.

Reaction Rates

The scalar distributions in the flame, when compared with analogous flamelet profiles, indicate that upstream interactions occur 1) in the rich region with the consequence of enhanced heat release, 2) at the nonpremixed interface leading to higher heat release through H_2 and CO oxidation, and 3) in the lean region where methane consumption occurs despite the local equivalence ratios being well below the lean flammability limit.

The flame interactions can be visualized through contour plots of the rates of four significant reactions presented in Figs. 9a–9d. The reaction set includes the important initiation reactions 1) $CH_4 + H \Leftrightarrow CH_3 + H_2$ (in the premixed flame) and 2) $H + O_2 \Leftrightarrow OH + O$

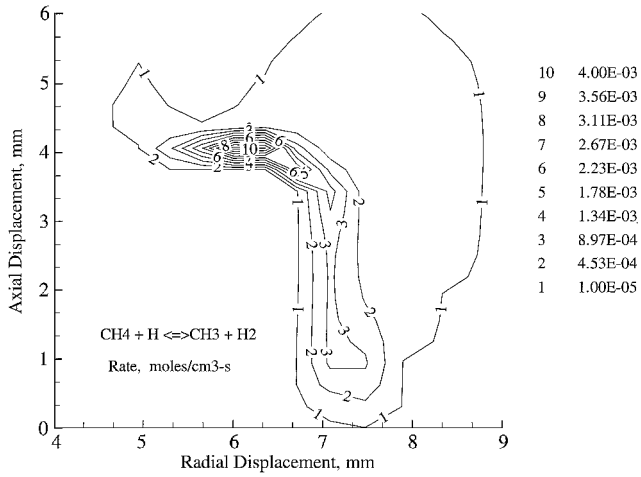

a) $CH_4 + H \Leftrightarrow CH_3 + H_2$

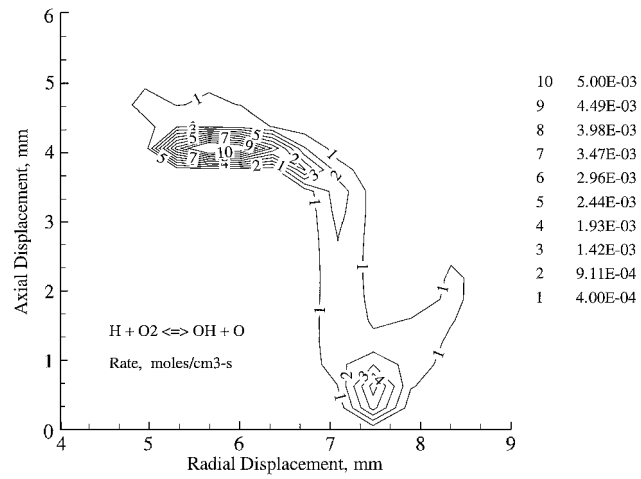

b) $H + O_2 \Leftrightarrow OH + O$

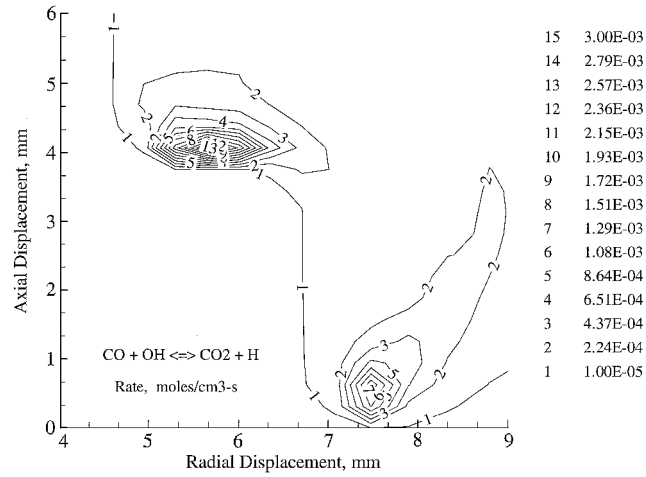

c) $H_2 + OH \Leftrightarrow H_2O + H$

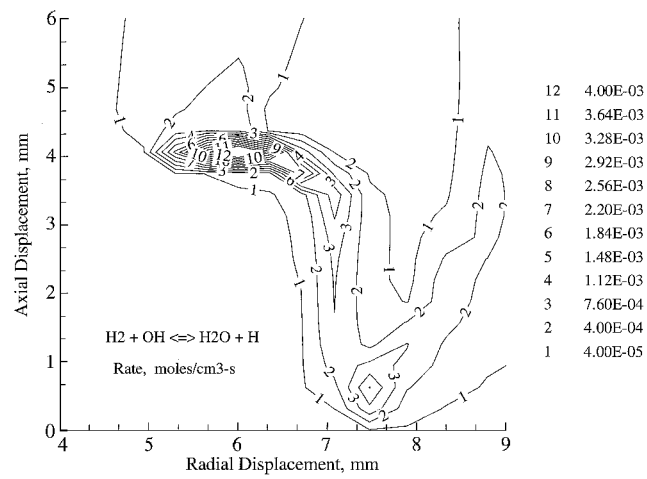

d) $CO + OH \Leftrightarrow CO_2 + H$

Fig. 9 Contours of the reaction rates.

(throughout the flame, except in the very lean region where the reverse reaction dominates) and the oxidation reactions 3) $H_2 + OH \Leftrightarrow H_2O + H$ and 4) $CO + OH \Leftrightarrow CO_2 + H$. In Fig. 9a we bound the methane-consumption contours of reaction 1 between two orders of magnitude, i.e., 4×10^{-3} and 10^{-5} moles $cm^{-3}\ s^{-1}$. Comparing Figs. 7b, 8a, and 9a, we note that the bulk of methane is consumed in the rich premixed flame. This flame (RPF) has an inverted L shape and has three distinct local sources, one distributed over each leg (one being around $z \approx 4$ mm, and the other close to $r \approx 7$ mm), with a third located at their intersection. Upon comparing Figs. 5, 8b, and 9a, we observe that this reaction proceeds at a smaller rate (5×10^{-4}–10^{-5} moles $cm^{-3}\ s^{-1}$) in both the lean and rich regions. This allows us to identify a lean premixed flame (LPF) around the location $z = 4.5$ mm and $r = 5$ mm.

Figure 9b presents the contours of oxygen consumption through reaction 2 bounded over one order of magnitude from 4×10^{-4} and 5×10^{-3} moles $cm^{-3}\ s^{-1}$. The nonpremixed flames can be visualized through the contours of the oxidation reactions, namely, reactions 3 and 4, which are presented in Figs. 9c and 9d. There are two distinct nonpremixed flames situated in a manner similar to that depicted schematically in Fig. 4. Figures 5, 8b, and 9d indicate that small levels of H_2 consumption occur in the rich region, in accord with the scalar distribution presented in Fig. 7c. Comparing Figs. 5, 9c, and 9d, we note that the maximum reaction rate contours of reactions 3 and 4 lie around $\xi \approx 0.45$.

In summary, the reaction rate profiles show a spatially thin rich premixed flame, two spatially broad NFs at either wing of the RPF, and an LPF stabilized by heat and mass transport toward the oxidizer-rich center. Comparing Figs. 9b and 9c, we observe a triple flame stabilized downstream of the innermost duct consisting of an RPF, LPF, and NF, with a structure similar to that shown in the schematic diagram of Fig. 2, but with upstream interactions between the three flames. The synergistic interactions between the inner and outer layers observed in the present study and the formation of complex composite flames underline the potential for further studies on these interactions and the ensuing flame structure.

Conclusions

Numerical simulations were conducted to investigate the flame structure of a transient partially premixed flame established by introducing a fuel-rich (CH_4–air) annular jet sandwiched between an axisymmetric air jet (on the inside) and coflowing air (on the outside). The flame structure was compared with that of an equivalent steady partially premixed flamelet by examining the scalar profiles of temperature and major species (CH_4, O_2, CO_2, H_2O, CO, H_2, and OH) profiles, as well as key reaction rate profiles, in a modified mixture fraction coordinate.

The structure of the axisymmetric partially premixed flame consists of an inner premixed flame that is synergistically coupled with an outer diffusion flame. The inner flame provides the intermediate fuels, namely, CO and H_2, to the outer flame, which in return provides the preheating and radical pool to initiate CH_4 consumption in the inner layer. The intermediate fuels CO and H_2 are oxidized by hydroxyl radicals in the nonpremixed flame through the major heat-release reactions and form CO_2 and H_2O. The H atoms, produced through oxidation of CO and H_2, react with O_2 in the outer layer to form OH and are also transported (through diffusion) to react with CH_4 in the inner layer.

The detailed structure of an axisymmetric flame has been compared with that of an equivalent partially premixed flamelet with respect to a modified conserved scalar $\xi = (Z - Z_1)/(Z_r - Z_1)$. The objective was to examine the effects of multidimensionality that might induce spatially and temporally varying strain rates and complex flow chemistry interactions due to differential transport of enthalpy and radicals. The comparison indicates that although the flame structure is similar to that of an equivalent flamelet, system-specific effects can induce the formation of complex composite flames. However, in general, regardless of specific transport and chemistry effects, it is possible to establish state relationships for flame structure in terms of the temperature and species concentration profiles.

The scalar distributions in the flame, when compared with analogous flamelet profiles, indicate that upstream interactions occur 1) in the rich region with the consequence of enhanced heat release, 2) at the nonpremixed interface leading to higher heat release through H_2 and CO oxidation, and 3) in the lean region where methane consumption occurs despite the local equivalence ratios being well below the lean flammability limit. The departures of the unsteady scalar profiles from their flamelet counterparts in a narrow region on the rich side are most likely due to system-specific transport effects, as discussed earlier. This information can prove useful in turbulent combustion modeling.

The reaction rate profiles show a spatially thin (composite) rich premixed flame, two spatially broad nonpremixed flames at either wing of the rich premixed flame, and a lean premixed flame stabilized by heat and mass transport toward the oxidizer-rich center.

Acknowledgments

This research was partially supported by the National Science Foundation's Combustion and Plasma Systems Program for which Farley Fisher is the Program Director.

References

[1]Libby, P. A., and Economos, C., "A Flame Zone Model for Chemical Reaction in a Laminar Boundary Layer with Application to the Injection of Hydrogen-Oxygen Mixtures," *International Journal of Heat and Mass Transfer*, Vol. 6, 1963, pp. 113–128.

[2]Yamaoka, I., and Tsuji, H., "The Structure of Rich Fuel-Air Flames in the Forward Stagnation Region of a Porous Cylinder," *Fifteenth Symposium (International) on Combustion*, Combustion Inst., Pittsburgh, PA, 1974, pp. 637–644.

[3]Yamaoka, I., and Tsuji, H., "Structure Analysis of Rich Fuel-Air Flames in the Forward Stagnation Region of a Porous Cylinder," *Sixteenth Symposium (International) on Combustion*, Combustion Inst., Pittsburgh, PA, 1976, pp. 1145–1154.

[4]Yamaoka, I., and Tsuji, H., "An Experimental Study of Flammability Limits Using Counterflow Flames," *Seventeenth Symposium (International) on Combustion*, Combustion Inst., Pittsburgh, PA, 1978, pp. 843–855.

[5]Rogg, B., Behrendt, F., and Warnatz, J., "Turbulent Nonpremixed Flames in Partially-Premixed Diffusion Flamelets with Detailed Chemistry," *Twenty-First Symposium (International) on Combustion*, Combustion Inst., Pittsburgh, PA, 1986, pp. 1533–1541.

[6]Hamins, A., Thridandam, H., and Seshadri, K., "Structure and Extinction of a Counterflow Partially-Premixed, Diffusion Flame," *Chemical Engineering Science*, Vol. 40, 1985, pp. 2027–2038.

[7]Smooke, M. D., Seshadri, K., and Puri, I. K., "The Structure and Extinction of Partially Premixed Flames Burning Methane in Air," *Twenty-Second Symposium (International) on Combustion*, Combustion Inst., Pittsburgh, PA, 1988, pp. 1555–1563.

[8]Law, C. K., Li, T. X., Chung, S. H., Kim, J. S., and Zhu, D. L., "On the Structure and Extinction Dynamics of Partially-Premixed Flames: Theory and Experiment," *Combustion Science and Technology*, Vol. 64, 1989, pp. 199–232.

[9]Rokke, N. A., Hustad, J. E., and Sønju, O. K., "A Study of Partially-Premixed Unconfined Propane Flames," *Combustion and Flame*, Vol. 97, 1994, pp. 88–106.

[10]Yule, A. J., Chigier, N. A., Ralph, S., Boulderstone, R., and Ventura, J., "Combustion-Transition Interaction in a Jet Flame," *AIAA Journal*, Vol. 19, 1981, pp. 752–760.

[11]Shu, Z., Aggarwal, S. K., Katta, V. R., and Puri, I. K., "Flame-Vortex Dynamics in an Inverse Partially Premixed Combustor: The Froude Number Effects," *Combustion and Flame*, Vol. 111, 1997, pp. 276–295.

[12]Shu, Z., Aggarwal, S. K., Katta, V. R., and Puri, I. K., "A Numerical Investigation of the Flame Structure of an Unsteady Inverse Partially-Premixed Flame," *Combustion and Flame*, Vol. 111, 1997, pp. 296–311.

[13]Peters, N., "Flame Calculations with Reduced Mechanisms—An Outline," *Reduced Kinetic Mechanisms for Applications in Combustion Systems*, Vol. m15, Lecture Notes in Physics, edited by N. Peters and B. Rogg, Springer–Verlag, Berlin, 1993, pp. 3–14.

[14]Sivathanu, Y. R., and Faeth, G. M., "Generalized State Relationships for Scalar Properties in Nonpremixed Hydrocarbon/Air Flames," *Combustion and Flame*, Vol. 82, 1990, pp. 211–230.

[15]Kee, R. J., Miller, J. A., and Warnatz, J. A., "Fortran Program Package for the Evaluation of Gas-Phase Viscosities, Conductivities, and Diffusion Coefficients," Sandia National Lab., Rept. SAND83-8209, Livermore, CA, March 1983.

[16]Leonard, B. P., "A stable and Accurate Convective Modelling Procedure Based on Quadratic Upstream Interpolation," *Computer Methods in Applied Mechanics and Engineering*, Vol. 19, 1979, pp. 59–98.

[17]Spalding, D. B., "A Novel Finite Difference Formulation for Difference Expressions Involving Both First and Second Derivatives," *International Journal of Numerical Methods in Engineering*, Vol. 4, 1972, pp. 551–559.

[18] Katta, V. R., Goss, L. P., and Roquemore, W. M., "Effect of Nonunity Lewis Number and Finite-Rate Chemistry on the Dynamics of a Hydrogen-Air Jet Diffusion Flame," *Combustion and Flame*, Vol. 96, 1994, pp. 60–74.

[19] Takahashi, F., and Katta, V. R., "Numerical Experiments on the Vortex Flame Interactions in a Jet Diffusion Flame," *Journal of Propulsion and Power*, Vol. 11, 1995, pp. 170–177.

[20] Aggarwal, S. K., Park, T. W., and Katta, V. R., "Unsteady Spray Behavior in a Heated Jet Shear Layer—Droplet-Vortex Interactions," *Combustion Science and Technology*, Vol. 113, 1996, pp. 429–438.

[21] Patadia, H., "Transient Structure of Methane-Air and Methanol-Air Diffusion Flames," M.S. Thesis, Dept. of Mechanical Engineering, Univ. of Illinois, Chicago, IL, 1995.

[22] Seshadri, K., Puri, I., and Peters, N., "Experimental and Theoretical Investigations of Partially Premixed Diffusion Flames at Extinction," *Combustion and Flame*, Vol. 61, 1985, pp. 237–249.

[23] Peters, N., and Williams, F. A., "The Asymptotic Structure of Stoichiometric Methane-Air Flames," *Combustion and Flame*, Vol. 68, 1987, pp. 185–207.

[24] Seshadri, K., and Peters, N., "The Inner Structure of Methane-Air Flames," *Combustion and Flame*, Vol. 81, 1990, pp. 96–118.

[25] Seshadri, K., and Göttgens, J., "The Structure of the Oxidation Layer for Stoichiometric and Lean Methane-Air Flames," *Reduced Kinetic Mechanisms and Asymptotic Approximations for Methane-Air Flames*, edited by M. D. Smooke, Springer–Verlag, New York, 1991, pp. 111–136.

[26] Bui-Pham, M., Seshadri, K., and Williams, F. A., "The Asymptotic Structure of Premixed Methane-Air Flames with Slow CO Oxidation," *Combustion and Flame*, Vol. 89, 1992, pp. 343–362.

[27] Lee, K. Y., Cha, D. J., Hamins, A., and Puri, I. K., "An Investigation of the Role of Radiative Thermal Loss in Inhibited Counterflow Flames," *Combustion and Flame*, Vol. 104, 1996, pp. 27–40.

[28] Sohrab, S. H., Ye, Z. Y., and Law, C. K., "An Experimental Investigation on Flame Interaction and the Existence of Negative Flame Speeds," *Twentieth Symposium (International) on Combustion*, Combustion Inst., Pittsburgh, PA, 1984, pp. 1957–1965.

[29] Bray, K. N. C., and Peters, N., "Laminar Flamelets in Turbulent Flames," *Turbulent Reacting Flows*, edited by P. A. Libby and F. A. Williams, Academic, London, 1994, pp. 63–113.

[30] Rogg, B., "RUN-1DS: A Computer Program for the Simulation of One-Dimensional Chemically Reacting Flows," Univ. of Cambridge, Rept. CUED/A-THERMO/TR39, Cambridge, England, UK, April 1991.

[31] Rogg, B., "Numerical Modeling and Computation of Reactive Stagnation-Point Flows," *Computers and Experiments in Fluid Flow*, edited by G. M. Carlomagno and C. A. Brebbia, Springer–Verlag, Berlin, 1989, pp. 75–85.

[32] Miller, J. A., and Bowman, C. T., "Mechanism and Modeling of Nitrogen Chemistry in Combustion," *Progress in Energy and Combustion Science*, Vol. 15, 1989, pp. 287–338.

[33] Tseng, L.-K., Gore, J. P., Puri, I. K., and Takeno, T., "C_2H_2 and C_2H_4 Concentrations in Partially Premixed Methane/Air Flames," *Twenty-Sixth Symposium (International) on Combustion*, Combustion Inst., Pittsburgh, PA, 1996, pp. 993–999.

[34] Norton, T. S., Smyth, K. C., Miller, J. H., and Smooke, M. D., "Comparison of Experimental and Computed Species Concentration and Temperature Profiles in Laminar Two-Dimensional Methane/Air Diffusion Flames," *Combustion Science and Technology*, Vol. 90, 1993, pp. 1–34.

G. M. Faeth
Editor-in-Chief